Measuring Ca^{2+}-Induced Structural Changes in Lipid Monolayers: Implications for Synaptic Vesicle Exocytosis

Sajal Kumar Ghosh,[†] Simon Castorph,[†] Oleg Konovalov,[‡] Tim Salditt,[†*] Reinhard Jahn,[§] and Matthew Holt[§¶*]
[†]Institute for X-Ray Physics, University of Göttingen, Göttingen, Germany; [‡]European Synchrotron Radiation Facility, Grenoble, France; [§]Department of Neurobiology, Max Planck Institute for Biophysical Chemistry, Göttingen, Germany; and [¶]VIB Center for the Biology of Disease, Katholieke Universiteit Leuven, Leuven, Belgium

ABSTRACT Synaptic vesicles (SVs) are small, membrane-bound organelles that are found in the synaptic terminal of neurons. Although tremendous progress has been made in understanding the protein machinery that drives fusion of SVs with the presynaptic membrane, little progress has been made in understanding changes in the membrane structure that accompany this process. We used lipid monolayers of defined composition to mimic biological membranes, which were probed by x-ray reflectivity and grazing incidence x-ray diffraction. These techniques allowed us to successfully monitor structural changes in the membranes at molecular level, both in response to injection of SVs in the subphase below the monolayer, as well as to physiological cues involved in neurotransmitter release, such as increases in the concentration of the membrane lipid PIP_2, or addition of physiological levels of Ca^{2+}. Such structural changes may well modulate vesicle fusion in vivo.

INTRODUCTION

Synaptic vesicles (SVs) are secretory organelles that store neurotransmitters in presynaptic nerve endings. Following action potential invasion of the nerve terminal, the plasma membrane is depolarized, leading to the opening of voltage-gated Ca^{2+} channels in the plasma membrane. The accompanying rise in intracellular Ca^{2+} leads to the fusion (exocytosis) of synaptic vesicles with the plasma membrane, resulting in the release of neurotransmitter (1–3).

The last two decades have seen tremendous progress in our understanding of the exocytic process at the molecular level. A whole network of proteins has been identified that are thought to play key roles in the process. In particular, attention has been focused on the so-called SNARE proteins, which are thought to drive membrane fusion, and a detailed, mechanistic molecular model of how these proteins function in membrane fusion has been proposed (which is discussed in the review by Jahn et al. (4)).

Perhaps unsurprisingly, our protein-centric view of the fusion process has meant that the role of lipids in the process (and by extension membranes and membrane structure) has been largely ignored. A case in point is the plasma membrane lipid phosphatidylinositol 4,5-bisphosphate (PIP_2). Although a minor component of the total membrane lipid, PIP_2 is known to be essential for exocytosis and is found specifically enriched at sites of vesicle fusion (5,6). To date, the role of PIP_2 in exocytosis has mainly been attributed to its function as an effector lipid for the vesicular protein synaptotagmin. Synaptotagmin is thought to act as a molecular bridge between the vesicle and plasma membranes, facilitating SNARE protein interactions that drive the fusion reaction (4).

However, multivalent cations such as Ca^{2+} are also known to directly interact with membranes, altering the electrostatic environment with potential consequences for the biochemical and physiological activities of the membrane, including protein function (7–13). For instance, PIP_2 is a strongly anionic lipid, with a headgroup possessing 3–5 net negative charges (14), which, depending on orientation and flexibility, may well interact with Ca^{2+} to produce highly localized membrane effects. Therefore, it is conceivable that structural changes in the plasma membrane induced by Ca^{2+} binding directly to PIP_2 at the release site may play an important role in modifying the local membrane environment, thus modulating synaptic vesicle exocytosis. However, the structural basis of how Ca^{2+} and PIP_2 function at the fusion site has been largely ignored, at least in part because of the overall complexity of biological systems and a lack of suitable experimental methods. We have recently taken a reductionist approach to such problems, using a Langmuir trough-based system to produce membrane monolayers of defined lipid composition, which can be investigated under precisely controlled conditions by x-ray reflectivity and grazing incidence x-ray diffraction (15). In this work, we use this approach to make a quantitative study of membrane structure in response to Ca^{2+} and PIP_2 (16).

As in any biophysical model system, the advantage to probe structural changes at the molecular level comes at a price. Reducing the complexity of the synaptic terminal to a two-component monolayer system facing an aqueous suspension of SVs limits the conclusions to be drawn. However, the rationale of this study is as follows: the structure of the fatty acids, even if different from the real system, is used as a structural reporter for the changes in the headgroup region (lateral pressure, electrostatics), because the chain reorganizes after interaction of the headgroup

Submitted August 12, 2011, and accepted for publication January 5, 2012.
*Correspondence: tsaldit@gwdg.de or Matthew.Holt@cme.vib-kuleuven.be
Editor: Ka Yee Lee.
© 2012 by the Biophysical Society
0006-3495/12/03/1394/9 $2.00
doi: 10.1016/j.bpj.2012.01.006

moieties with either small ions or SV proteins to lower the free energy. If these changes are significant in the monolayer model system, they are most likely also important in the biological membrane, even if the starting configuration is different in terms of composition and fluidity.

What we observe here is a significant Ca^{2+}-dependent reorganization of the acyl chains as well as corresponding changes in the electron density profile, in particular in the presence of PIP_2. Based on these results, we speculate that changes in membrane structure produced by direct cation binding to lipids may regulate Ca^{2+}-dependent synaptic vesicle fusion with the plasma membrane. We believe these results call for a revision of the current protein-centered view of neurotransmitter release, to incorporate an active role for the lipid microenvironment during release.

MATERIALS AND METHODS

Lipid monolayers were prepared from the lipids dipalmitoyl-*sn*-glycero-3-phosphatidylcholine (DPPC) and phosphatidylinositol-4,5-bisphosphate (PIP_2). To prepare lipid monolayers at an air-water interface, we used a custom-made shallow Langmuir trough, equipped with a single movable Teflon (DuPont, Wilmington, DE) barrier, available at ID10B of the European Synchrotron Radiation Facility (Grenoble, France). Each monolayer was exposed multiple times to collect the data at various salt concentrations in the subphase (see below). The special choice of the majority lipid DPPC in the monolayer follows from the fact that monolayer formation and chain ordering in this lipid is particularly easy, well described, and robust. The ordering in the saturated fatty acids corresponds more to a bilayer's gel phase than to a bilayer's fluid phase. Measurements on both the DPPC and DPPC/PIP_2 monolayers were carried out at a temperature of 18°C, which is below the chain-melting temperature of DPPC. $CaCl_2$ and/or synaptic vesicles were subsequently injected into the subphase using a microloader. The 1 M $CaCl_2$ stock was added sequentially into the subphase to achieve the desired final Ca^{2+} concentration; in a first step the Ca^{2+} concentration was raised to 1 μM, and for subsequent experiments further Ca^{2+} was added to reach effective concentrations of 10 μM and 30 μM, respectively. Synaptic vesicles were purified from rat brain, as described in Takamori et al. (1), through differential centrifugation, sucrose density centrifugation, and size-exclusion chromatography. Synaptic vesicles were routinely used at a final concentration of ~1.5 g/L. Fig. 1 *A* illustrates the experimental systems used. The details of the preparation methods concerning both the monolayer and the SVs, as well as the experimental parameters, are given in the Supporting Material.

Grazing incidence x-ray diffraction (GIXD) and x-ray reflectivity measurements on monolayers were carried out using the undulator beamline ID10B at the European Synchrotron Radiation Facility. Briefly, a monochromatized x-ray beam was deflected by a downstream mirror to set the incident angle (α_i) onto the interface. This angle was taken to be $0.8\alpha_c$, where α_c is the critical angle for total external reflection at an air-water interface. To collect the diffracted beam from the sample, a linear position-sensitive detector (150 mm long Gabriel detector; European Molecular Biology Laboratory, Grenoble, France) was used (see the Supporting Material for details).

A two-dimensional crystalline arrangement of lipid molecules in the monolayer plane can be calculated from the observed d-spacings using the horizontal components q_{xy}^{hk} of the momentum transfer vector. The primitive unit cell parameters a and b provide the area per chain (A_I). Further, the projected area of the chains gives a measure of the area in an untilted phase and is obtained by $A_{II} = A_I\cos(\tau)$, where τ is a tilt in the hydrocarbon chain from the layer normal (Fig. 1 *A*). It can be calculated from the peak positions of q_{xy}^{hk} and the vertical component q_z^{hk}. X-ray reflectivity experiments were performed at a surface pressure of 30 mN/m. The x-ray analysis is detailed in the Supporting Material.

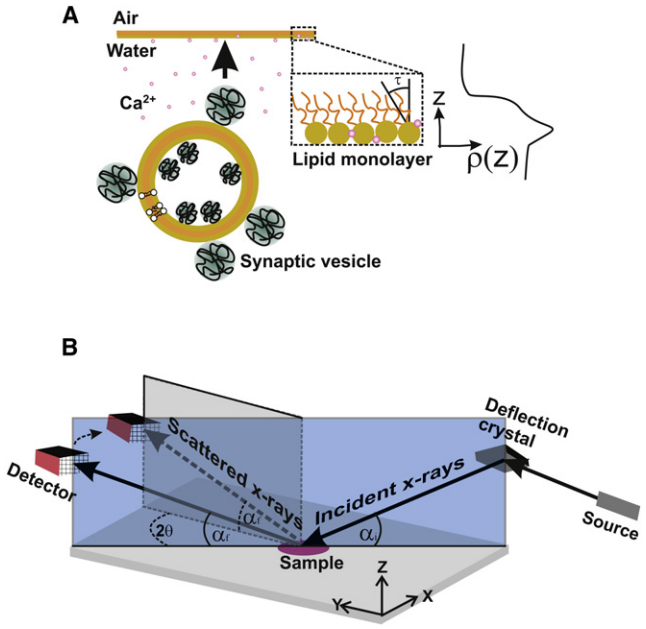

FIGURE 1 Schematics of the experimental systems used. (*A*) Lipid monolayers were formed at an air-water interface. X-ray reflectivity was used to measure the electron density profile of the lipid layer (ρ(z)) in this system. GIXD was used to measure the tilt angle (τ) of the lipid acyl chains. Where necessary, defined amounts of Ca^{2+}, as well as synaptic vesicles, were introduced into the subphase. (*B*) The equipment used for x-ray scattering experiments. For reflectivity, the incident angle (α_i) = reflected angle (α_f) with $2\theta = 0$. For GIXD, $\alpha_i < \alpha_c$ and $2\theta \neq 0$, where α_c is the critical angle at the air-water interface. Note that the z axis is parallel to the sample normal.

RESULTS

X-ray reflectivity measurements from lipid monolayers

To begin, we used the technique of x-ray reflectivity to obtain the laterally averaged electron density profile for membranes of defined composition, as a function of the interface normal (*z axis* in Fig. 1). This profile can be used to deduce structural parameters of the membrane under investigation. We analyzed reflectivity data using kinematical approximation, with the electron density profile modeled using two boxes. One box was used to describe the hydrophilic headgroup, while the other described the hydrocarbon chain of the lipid. The electron densities of the subphase and the air were taken to be $0.334e^-/Å^3$ and zero, respectively. The capillary wave roughness of the water surface was fixed at 3.2 Å.

Baseline measurements of basic membrane parameters were obtained using a pure DPPC monolayer as a reference. Fig. 2 shows reflectivity data obtained from such a monolayer before and after injection of increasing amounts of

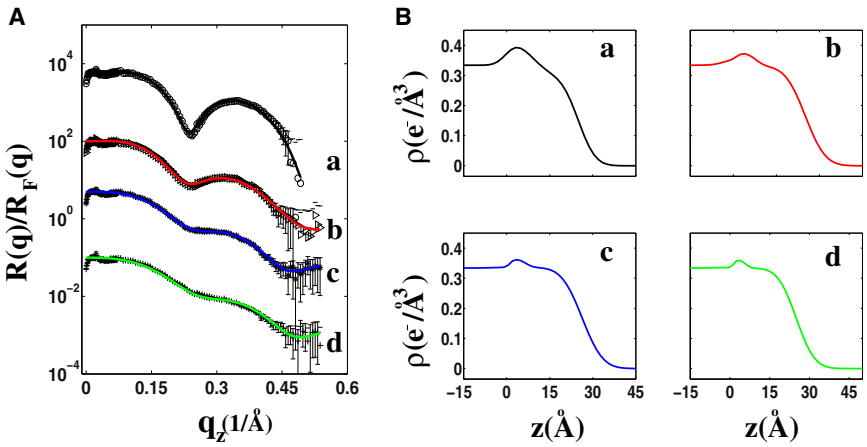

FIGURE 2 X-ray reflectivity measurements made from DPPC monolayers. (*A*) Measurements were made from pure DPPC monolayers (*a*, ○), and DPPC monolayers with increasing concentrations of Ca^{2+} in the subphase: 1 μM (*b*, ▷), 10 μM (*c*, *), and 30 μM (*d*, +). For clarity, the curves have been shifted vertically. (*B*) The corresponding electron density profiles obtained from the best fits (given by the *solid lines* in panel *A*).

Ca^{2+}. In the electron density profiles, the peaks correspond to the headgroup regions of the measured monolayers. In the pure DPPC monolayer, the box model fit gave a headgroup size of 8.75 Å (box model), and an overall lipid thickness of 25 Å (headgroup plus chains). The box-model density value of the headgroup was $0.43e^{-}/Å^3$. Note, however, that this value is not reached by the actual curve, due to convolution (smearing) by roughness. The hydrocarbon-chain electron density was $0.3e^{-}/Å^3$, visible as a shoulder in the profile between density maximum and air. These values are in agreement with previous measurements (15,17). Injection of $CaCl_2$ into the subphase led to a reduction in amplitude of the modulation in the respective reflectivity curves. Subsequent analysis showed that the amplitude of this reflectivity modulation depends critically on the headgroup contrast. Best fits to the data showed the electron density of the headgroup decreased monotonically, being $0.34e^{-}/Å^3$ at a final concentration of 30 μM $CaCl_2$ in the subphase ($\Delta\rho \sim 20\%$), with an overall headgroup size of 8.05 Å. In contrast, we found that the electron density of the lipid chain increased slightly to $0.32e^{-}/Å^3$.

The structural effect of adding PIP_2 into the monolayer is shown in Fig. 3. Interestingly, the electron density profile deduced from the best fit of the DPPC/PIP_2 data showed a slight decrease in the average electron density to $0.42e^{-}/Å^3$of the lipid headgroups compared to pure DPPC (15,18). Again, addition of $CaCl_2$ to the subphase caused a monotonic decrease in the headgroup electron density. At 30 μM $CaCl_2$, the density was $0.37e^{-}/Å^3$ ($\Delta\rho \sim 12\%$). Note that this effect is less than seen with the pure DPPC monolayer. However, the effect on lipid headgroup size was much more dramatic; the overall size decreased from 7.18 Å to 4.3 Å. Compared to the expected size for the headgroup density maximum, which is in the range of 5–9 Å (17,19), this is an extremely low and unrealistic value. Although we cannot rule out an artifact in the fit, we offer a more speculative explanation. If the lateral area in the membrane per headgroup decreases along with the chain tilt angle (see subsection below), this is likely concomitant with a change in headgroup orientation to a more vertical direction. Correspondingly, if the headgroup volume is more elongated along the z axis (Fig. 1), it will contribute less to the overall electron density ($\rho(z)$) (averaged in xy), effectively being invisible against the buffer background. Thus, we propose that the small remaining peak is related to a highly localized positioning of Ca^{2+} interconnecting the phosphate moieties of the headgroups. Note that the data analysis is based on a box model, with both the size and the electron density of the box as free fit parameters. The result for the PIP_2/Ca^{2+} samples thus yield a smaller box width and a smaller electron density with respect to DPPC/zero Ca^{2+}. Hence, the box is reduced, and stands out as a small maximum with respect to the semiinfinite slab of the buffer. To avoid misunderstandings, we point out that the box names (i.e., headgroup box) are based on the interpretation of the control measurement without Ca^{2+}. As the structural features evolve, the fitted model parameters change and the box designators are only nominal, but still serve as useful fiducials when discussing the profiles. To summarize, our results from x-ray reflectivity measurements show that PIP_2 and Ca^{2+} both alone and in combination are sufficient to induce profound structural changes in membranes.

GIXD measurements from lipid monolayers

To try and further understand the effects of PIP_2 and Ca^{2+} on membrane structure we turned to GIXD, which is an experimental technique that provides information on the lateral ordering of the acyl chains in lipid molecule at an air-water interface (which, for the purpose of analysis, effectively represent a two-dimensional crystalline structure).

Fig. 4 shows a representative set of contour plots from GIXD experiments performed on DPPC and DPPC/PIP_2 monolayers in the absence and presence of $CaCl_2$ in the subphase. In this type of plot, the intensity distributions along both the horizontal (q_{xy}) and vertical (q_z)

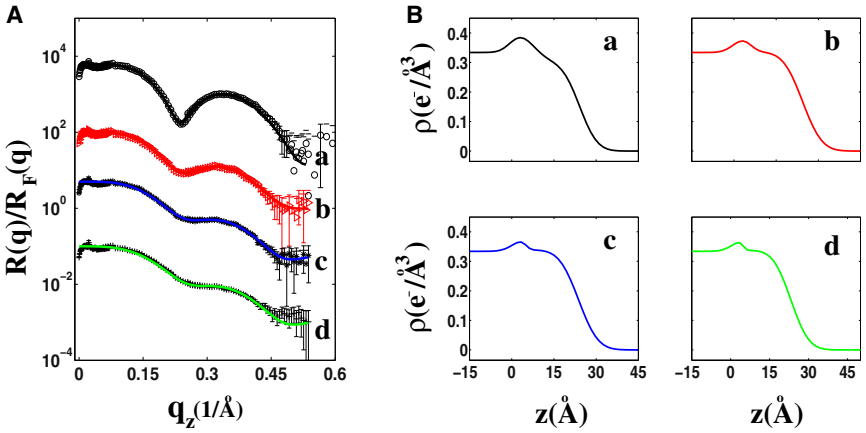

FIGURE 3 X-ray reflectivity measurements made from DPPC/PIP_2 monolayers. (*A*) X-ray reflectivity measurements from DPPC/PIP_2 monolayers (*a*, ○) and DPPC/PIP_2 monolayers with increasing concentrations of Ca^{2+} in the subphase: 1 μM (*b*, ▷), 10 μM (*c*, *), and 30 μM (*d*, +). For clarity, the curves have been shifted vertically. (*B*) The corresponding electron density profiles obtained from the best fits (given by the *solid lines* in panel *A*).

scattering vectors are resolved. For all our measured samples, the data projected on the q_{xy} axis (vertical integration of diffracted intensity) showed two Bragg peaks, which can be indexed as (11) and (02) of a centered rectangular unit cell (see Fig. 5). The presence of one out-of-plane Bragg rod at $q_z > 0$ indicates that the chains are tilted toward their nearest neighbors. However, it should be noted that such a centered rectangular lattice could also be interpreted as a distorted hexagonal lattice (20).

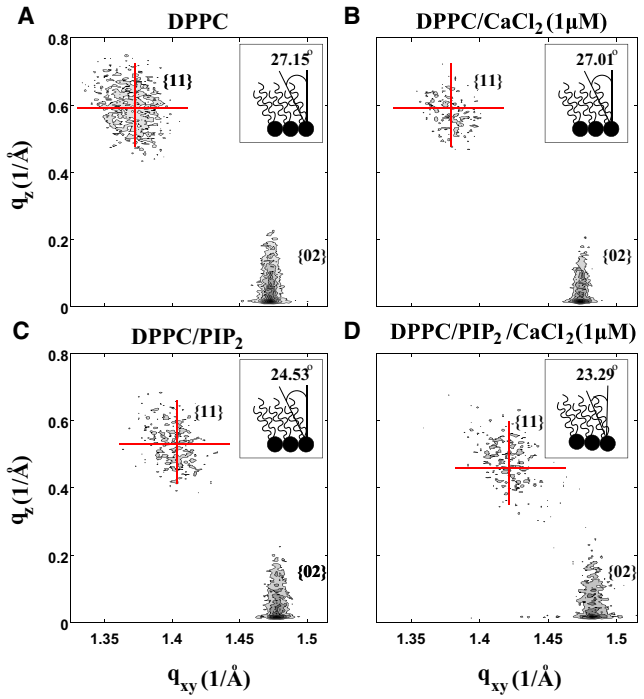

FIGURE 4 GIXD measurements made from DPPC and DPPC/PIP_2 monolayers. Contour plots of GIXD data from (*A*) a DPPC monolayer, (*B*) a DPPC monolayer with 1 μM Ca^{2+} in the subphase, (*C*) a DPPC/PIP_2 monolayer, and (*D*) a DPPC/PIP_2 monolayer with 1 μM Ca^{2+} in the subphase. (*Crosses*) Position of the {11} peak. (*Inset*) Averaged tilt angle of the lipid acyl chains under the corresponding conditions.

For pure DPPC monolayers, the lattice parameters of the unit cell were found to be 5.42 Å and 8.54 Å, equating to an area of 23.11 $Å^2$ for each chain. The calculated tilt angle of the lipid chains (27.15°) was lower than the value previously reported (~30°) when using an aqueous subphase of ultrapure water (21). In contrast, the buffer used as the subphase in our study contained 150 mM KCl, 25 mM HEPES (pH 7.40 KOH), and 1 mM DTT, which we assume to account for this slight difference. Addition of $CaCl_2$ to the subphase caused significant structural changes in the lipid monolayer. Although two Bragg peaks could still be observed (indicating a similar unit cell structure), the lattice parameters were decreased slightly, resulting in a concomitant decrease in the area occupied by each acyl chain (see Fig. 5 and Table 1). Furthermore, we observed a monotonic

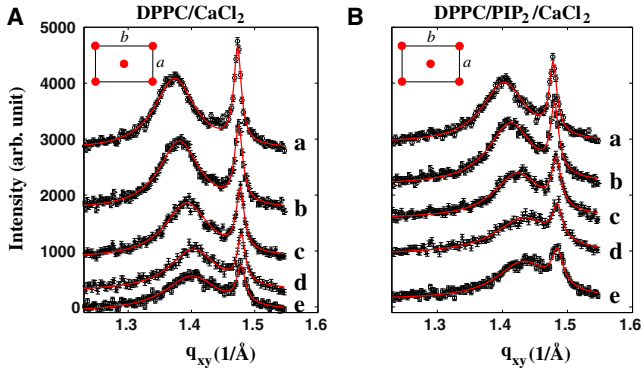

FIGURE 5 Diffraction peaks in the horizontal plane derived from GIXD measurements on monolayers. The data correspond to a scan along q_{xy} with vertically integrated intensity (sum over all position-sensitive detector channels), so that all peaks show up. Diffraction peaks were obtained for (*A*) pure DPPC and (*B*) DPPC/PIP_2 monolayers. Measurements were made in the absence of Ca^{2+} (*a*, ○), and with increasing concentrations of Ca^{2+} in the subphase: 1 μM (*b*, ▷), 10 μM (*c*, *), and 30 μM (*d*, +). Reversibility of Ca^{2+}-induced changes was tested by adding 10 mM of the Ca^{2+} chelator EGTA at the end of the experiment (*e*, □). The Bragg peaks were fitted to two Lorentzians (*solid lines*). (*Inset*) Hydrocarbon chains of the lipid molecules in the monolayers could be described by a centered rectangular unit cell.

TABLE 1 Structural parameters derived from the in-plane Bragg peaks and out-of-plane Bragg rods obtained from GIXD experiments on lipid monolayers of various compositions

Sample	d_{11} (Å)	d_{02} (Å)	a (Å)	b (Å)	A_I (Å^2)	A_{II} (Å^2)	L_{11} (Å)	L_{02} (Å)	τ (deg)
DPPC	4.58	4.27	5.42	8.54	23.11	20.57	72.5	447.0	27.2
DPPC/1 μM $CaCl_2$	4.55	4.23	5.39	8.52	22.92	20.42	72.7	411.3	27.0
DPPC/10 μM $CaCl_2$	4.50	4.25	5.31	8.51	22.58	20.38	66.0	404.9	25.5
DPPC/30 μM $CaCl_2$	4.47	4.24	5.27	8.49	22.37	20.27	61.8	398.7	25.0
DPPC/30 μM $CaCl_2$/10 mM EGTA	4.47	4.25	5.26	8.51	21.26	20.30	54.5	381.2	24.9
DPPC/PIP_2	4.47	4.25	5.26	8.51	22.38	20.36	69.2	455.0	24.5
DPPC/PIP_2/1 μM $CaCl_2$	4.44	4.25	5.21	8.49	22.14	20.30	67.1	408.1	23.3
DPPC/PIP_2/10 μM $CaCl_2$	4.40	4.24	5.15	8.48	21.82	20.16	64.4	367.9	22.5
DPPC/PIP_2/30 μM $CaCl_2$	4.34	4.23	5.06	8.46	21.40	20.31	51.9	348.5	18.5
DPPC/PIP_2/30 μM $CaCl_2$/10 mM EGTA	4.36	4.23	5.08	8.46	21.50	20.19	57.1	288.4	20.2
DPPC/PIP_2/SV	4.51	4.25	5.32	8.50	22.65	20.36	65.0	290.0	26.0
DPPC/PIP_2/SV/1 μM $CaCl_2$	4.45	4.24	5.22	8.49	22.18	20.20	52.4	378.4	24.4
DPPC/PIP_2/SV/10 μM $CaCl_2$	4.41	4.24	5.17	8.48	21.91	20.11	62.5	165.5	23.4
DPPC/PIP_2/SV/30 μM $CaCl_2$	4.34	4.24	5.05	8.48	21.43	19.89	46.7	195.0	21.7
DPPC/PIP_2/SV/30 μM $CaCl_2$/10 mM EGTA	4.40	4.24	5.15	8.48	21.82	19.99	53.4	122.6	23.7

The d-spacings are given by d_{11} and d_{02}. The dimensions of the rectangular unit cell are given by a and b. The area per chain and the projected area per chain are given by A_I and A_{II}, respectively. L_{11}, L_{02} are the domain sizes in the direction of q_{xy}^{11} and q_{xy}^{02}, and τ the tilt angle of the acyl chains.

decrease in the domain sizes L_{11} and L_{02}, in the directions of q_{xy}^{11} and q_{xy}^{02}, respectively, suggesting that Ca^{2+} reorganizes the packing of the lipid molecules in the monolayer, which is consistent with other structural parameters obtained from the data. Injection of the Ca^{2+} chelator EGTA into the subphase at the end of the experiment did not produce significant effects on the lattice structure of the acyl chains, although the domain sizes L_{11} and L_{02} were found to decrease further after EGTA addition.

Addition of PIP_2 to the monolayer caused the Bragg peaks to shift toward higher q_{xy} (see Figs. 4 and 5) (15). Interestingly, addition of Ca^{2+} to monolayers containing PIP_2 produced more profound structural changes when compared to DPPC alone. A full comparison of the various effects of PIP_2 and Ca^{2+} on monolayers of varying lipid compositions can be found in Table 1 and Fig. 6. Increasing the Ca^{2+} in the subphase resulted in a gradual decrease of both the lattice parameters describing the unit cell and the tilt angle of the acyl chains. At 30 μM Ca^{2+}, the tilt angle of the acyl chains was reduced by ~25% in the case of the DPPC/PIP_2 monolayer, compared to <10% in the case of pure DPPC. Interestingly, incorporation of PIP_2 into the membrane also caused a differential effect with regard to the effects of the Ca^{2+} chelator EGTA. In this case, injection of 10 mM EGTA into the subphase at the end of the experiment partially reversed the effects of the added Ca^{2+}; not only did the lattice parameters (and hence the area per lipid chain) increase, but we also observed a subsequent increase in the chain tilt angle from 18.47° to 20.20°.

Synaptic vesicle interaction and its influence on membrane structure

As both Ca^{2+} and PIP_2 are essential for synaptic vesicle exocytosis, an obvious question is the possible role of structural changes in the fusion process. Fortunately, standard protocols exist for the preparation of ultrapure synaptic vesicles from rat brain, in amounts sufficient to perform our Langmuir trough-based measurements.

Thus, we have injected isolated synaptic vesicles directly into the subphase of a monolayer prepared from DPPC and PIP_2. The interaction of SVs with the monolayer was evidenced by a bimodal increase in the interfacial pressure within a few minutes, followed by a much more gradual increase, as reported in Ghosh et al. (15). The Ca^{2+} concentration in the subphase was then progressively increased in the same fashion as in the experiments without SVs. Fig. 7 shows reflectivity data that was used to derive the laterally averaged electron density profiles for the measured

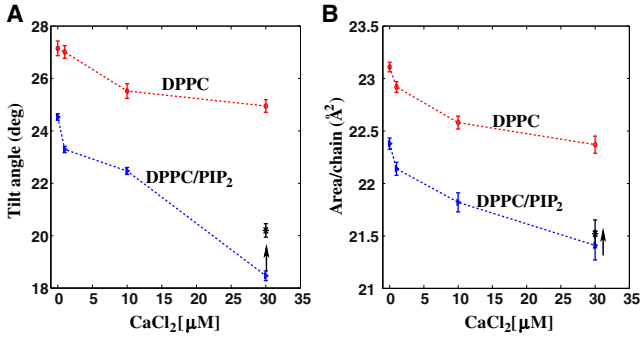

FIGURE 6 Summary of diffraction data obtained from monolayers with varying amounts of Ca^{2+} in the subphase. Effects of $CaCl_2$ injected in the subphase of monolayers consisting of DPPC (○) or DPPC/PIP_2 (▷). (*A*) Variation in tilt angle of the alkyl chains from the surface normal, and (*B*) the area occupied by each chain. The effect of EGTA on the DPPC/PIP_2 monolayer is represented by a single data point (*) and indicated (*arrow*). In this figure, the error bars are estimated from the confidence intervals of the optimized parameters that provided the best fits to the data shown in Fig. 5.

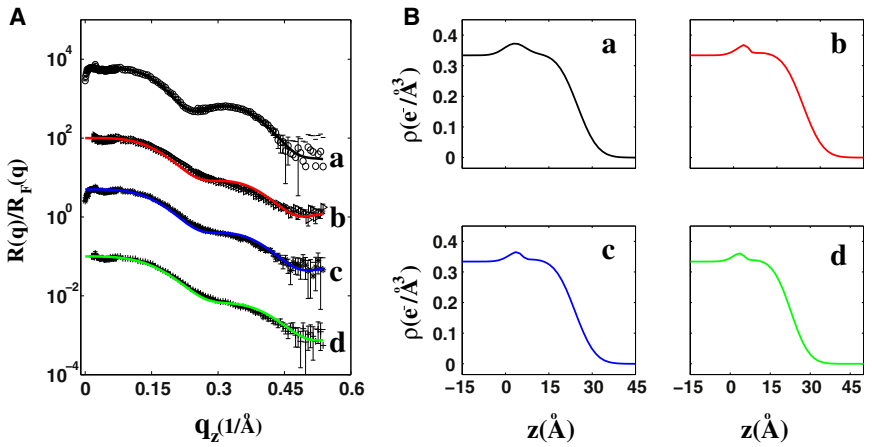

FIGURE 7 X-ray reflectivity measurements of DPPC/PIP_2 monolayers and the effect of synaptic vesicle addition. (*A*) X-ray reflectivity measurements from DPPC/PIP_2 monolayers with synaptic vesicles in the subphase both in the absence of Ca^{2+} (*a*, ○), and with increasing Ca^{2+} concentrations in the subphase: 1 μM (*b*, ▷), 10 μM (*c*, *), and 30 μM (*d*, +). For clarity, the curves have been shifted vertically. (*B*) Electron density profiles (obtained from the *solid lines* shown in panel *A*).

membranes. Addition of Ca^{2+} to the system resulted in structural changes to the monolayer, as shown by the distinct alterations in the electron density profiles we obtained. The structural changes followed a similar trend to that observed when synaptic vesicles were absent from the subphase: in the fit, both the width of the box (along *z*) attributed to the headgroup and its electron density decreased monotonically. At the highest concentration of Ca^{2+} in the subphase (30 μM), the box width was reduced to ~3 Å. As argued above, we attribute this to a change in headgroup tilt angle that in turn leads to an alteration in headgroup orientation. The small remaining peak would then be related to a highly localized positioning of Ca^{2+} interconnecting the phosphate moieties of the headgroups.

The structural basis of this rearrangement was investigated using GIXD to once again investigate the lateral ordering of the acyl chains in the lipid molecules. Results are shown in Figs. 8 and 9, and data are summarized in the lower panel of Table 1. The Bragg peaks obtained from the DPPC/PIP_2 monolayer, when synaptic vesicles were included in the subphase, showed a rectangular lattice structure, with an increased tilt angle compared to the DPPC/PIP_2 monolayer alone. Addition of increasing amounts of Ca^{2+} to the system resulted in structural changes to the monolayer, similar to the trend seen in both the DPPC and DPPC/PIP_2 systems. The tilt angle was found to decrease by ~12.5% at the highest Ca^{2+} concentration used (30 μM), which is less than the effect seen on the DPPC/PIP_2 system in the absence of synaptic vesicles. The domain sizes L_{11} and L_{02} were smaller than those without SVs for all Ca^{2+} concentrations. The addition of 10 mM EGTA to the subphase at the end of the experiment partly reversed the effects on chain tilt angle. The observed increase was ~2°, similar to that seen in the DPPC/PIP_2 system.

DISCUSSION

In this article, we have used x-ray reflectivity and grazing incidence x-ray diffraction to study the membrane structure at the initial stages of the fusion process, which we regard as equivalent to docking, the recruitment of SVs to the plasma membrane.

Lipid composition at the release site has a profound influence on membrane structure

A basic requirement for exocytosis is the membrane lipid PIP_2 (5,6). Interestingly, the addition of a small amount of PIP_2 was sufficient to induce a measurable structural effect in our system (Figs. 3–6). Hence, PIP_2 most likely plays an

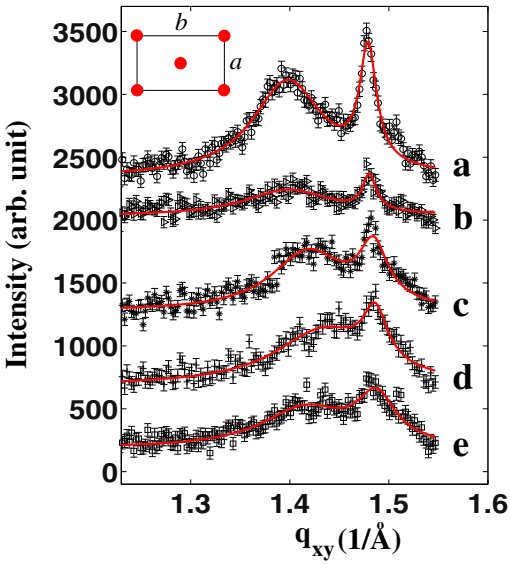

FIGURE 8 Diffraction peaks in the horizontal plane derived from GIXD measurements on monolayers in the presence of synaptic vesicles. Diffraction peaks were obtained for DPPC/PIP_2 monolayers with synaptic vesicles in the subphase both in the absence of Ca^{2+} (*a*, ○), and with increasing Ca^{2+} concentrations in the subphase: 1 μM (*b*, ▷), 10 μM (*c*, *), and 30 μM (*d*, +). Reversibility of Ca^{2+}-induced changes was tested by adding 10 mM of the Ca^{2+} chelator EGTA to the subphase at the end of the experiment (*e*, □). The Bragg peaks were fitted to two Lorentzians (*solid lines*). (*Inset*) Hydrocarbon chains of the lipid molecules in the monolayers could be described by a centered rectangular unit cell.

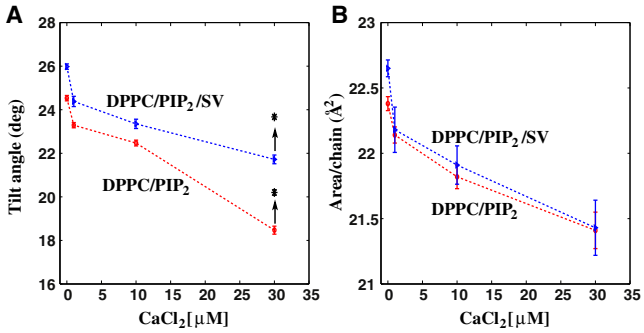

FIGURE 9 Summary of diffraction data obtained from monolayers incubated with synaptic vesicles with varying amounts of Ca^{2+} in the subphase. Effects of $CaCl_2$ injected into the subphase of a DPPC/PIP_2 monolayer either without (○) or with (▷) synaptic vesicles. (*A*) Variation in tilt angle of the alkyl chains from the surface normal, and (*B*) the area occupied by each chain. The effect of EGTA addition at the end of the experiment is represented by a single data point (*) and indicated (*arrow*).h

important role in shaping the structural microenvironment of the basic synaptic plasma membrane.

In vivo, exocytosis is also strictly dependent on increases in local Ca^{2+} at sites of vesicle fusion. A fact that is often overlooked is that PIP_2 is a highly charged molecule that could interact directly with Ca^{2+} at release sites. Even zwitterionic lipids are reported to undergo structural changes in their organization within membranes due to the presence of this ion (7,9,10). Although previous studies have used a variety of advanced physical techniques to investigate the electrostatic effects of Ca^{2+} on the arrangement of various membrane lipids, these studies have all used high concentrations of Ca^{2+} (12,13). In this study, we have measured the changes in monolayer structure that may occur at release sites under quasiphysiological conditions (22). Interestingly, we found profound effects on membrane structure induced by the electrostatic association of Ca^{2+} with phospholipid headgroups, both in x-ray reflectivity and grazing incidence x-ray diffraction measurements. PIP_2 is an anionic lipid with three-to-five net negative charges and is more likely to adsorb multivalent cations in the headgroup regions of the lipid film, with the effects scaling in proportion to the concentration of Ca^{2+} used. For example, in pure DPPC, the tilt angle τ decreases with Ca^{2+} concentration from 27.2° to 25.9° at a maximum concentration of 30 μM, while addition of PIP_2 enhances and shifts the dependence to the range of 24.5° to 18.5°.

In this work, we measured two main structural parameters; the tilt of the acyl chains and the area per lipid were measured as averages across an entire monolayer. These values are tightly interrelated. The interface properties (for example, electrostatic interactions, binding of macromolecules to the membrane surface, and the pressure of the film balance) contribute to fixing the area per lipid, while reorganization of the lipids through chain tilting serves to maximize van der Waals interactions. This effectively means the smaller the area per headgroup, the smaller the tilt angle. In other words, compensatory tilting of the acyl chains acts to maintain the hydrophobic core of the membrane. As discussed above, Ca^{2+} induces a significant reduction in both the area and tilt angle (Fig. 6), indicative of Ca^{2+}-induced compaction of the film; for example, by bridging the anionic phosphate groups of the lipid. This trend is partially counteracted by incubation of synaptic vesicles with the monolayer (Fig. 9), but is intensified with addition of PIP_2. A corresponding intensified effect with PIP_2 was manifested as a progressive reduction in the size of the headgroup box in the presence of PIP_2 and Ca^{2+}, suggesting that Ca^{2+} ions were effectively bridging-up the lipid molecules and compacting the lipids. Intuitively, this packing of lipids into a smaller unit cell resulted in a reduced area per chain and a reduction in tilt angle of the acyl chains as revealed by grazing incidence experiments.

Our results are in line both with numerical and experimental studies of the effects of cations on membrane structure. For instance, a molecular dynamics study has previously predicted a tight packing of zwitterionic lipids around Ca^{2+} ions, which leads to an increase in the ordering of the lipid chains (7). High-resolution neutron diffraction studies directly showed these Ca^{2+} ions to localize within the headgroup region of the DPPC bilayer in a lamellar phase (23), while NMR and IR spectroscopy studies suggested a conformational change in the polar region of the DPPC bilayer (10) and rearrangement in the carbonyl region of the lipid palmitoyloleoylphosphatidylcholine as a result of Ca^{2+} bridging (11).

Membrane structure and synaptic vesicle association

Unfortunately, it has proved difficult to unambiguously disentangle the structural changes in the lipid monolayer brought about by our various manipulations. The strong effects of Ca^{2+} and PIP_2 are likely brought about by simple electrostatic effects, resulting in "charge bridging" that compacts the membrane. The situation becomes more complex, however, when considering the effects seen on synaptic vesicle incubation—although two possibilities are readily apparent.

First, monolayer isotherm and interfacial pressure measurements have previously shown that isolated synaptic vesicles interact with lipid membranes in a Ca^{2+}-dependent manner (15), leading us to speculate on the possible insertion of synaptic vesicle-associated proteins into the monolayer. Our GIXD measurements of PIP_2-containing monolayers, incubated with synaptic vesicles, add considerable weight to this hypothesis. Although Ca^{2+} addition still leads to a reduction in the tilt of the acyl chains in this system, the effect is significantly less than seen in the absence of synaptic vesicles (Table 1).

Although we can make no direct judgment, it is tempting to speculate that synaptotagmin is most likely responsible

for mediating the interaction between vesicles and the membrane. Synaptotagmin is a major vesicle protein that contains tandem C2 domains—C2A and C2B (M. Koch and M. Holt, unpublished). Interestingly, synaptotagmin interacts with PIP_2 at concentrations of calcium required for transmitter release (24). It is thought that Ca^{2+} binding permits the hydrophobic residues at the tips of each C2 domain to penetrate the hydrophobic core of membranes; in particular, the C2B domain has been proposed to insert into the presynaptic membrane (6,25,26). This insertion is thought to induce a region of high positive curvature and strain in the membrane; this is relieved during the fusion process, reducing the overall energy cost of the reaction and favoring its completion (27–29).

Second, it is possible (although somewhat unlikely in our minds) that synaptic vesicles undergo partial fusion with the monolayers, which would lead to a rather undefined final state, with the DPPC film contaminated with synaptic vesicle lipids and proteins (also see later). Not withstanding the need for further investigation, the strong interfacial activity of SVs at the monolayer is clearly shown, as well as the corresponding modulation by Ca^{2+}. Note the significant reduction in the acyl chain domain size L_{02}, see second but last column in Table 1. Additionally, SV incubation with the monolayers decreased *L*02 by up to a factor of 2, when compared to the conditions of PIP_2 and Ca^{2+} alone. This would fit with the hypothesis of (partial) synaptic vesicle fusion that would lead to a rather undefined final state, with the DPPC film contaminated with synaptic vesicle lipids and presumably denatured proteins.

An active role for active membrane remodeling in the fusion process?

The strong interaction of PIP_2 and Ca^{2+} has potentially major implications for vesicle fusion in vivo. Synaptic vesicles fuse at defined sites on the plasma membrane defined partly by the presence of Ca^{2+} channels, which serve to elevate the local Ca^{2+} concentration to levels sufficient to trigger release. It is widely assumed that Ca^{2+} serves merely to function as a bridge between vesicular synaptotagmin and the PIP_2 in the plasma membrane. However, given the simple electrostatic nature of the interaction, we propose that at least a fraction of PIP_2 at the active zone rapidly binds the Ca^{2+} that enters the terminal during an action potential, a proposal that is consistent with the known kinetics of exocytosis (30). Experimentally, this idea is supported by the fact that even in our simplified system, structural parameters, such as the chain tilt angle, decrease more in the DPPC/PIP_2 system than in the pure DPPC system (25%–8%) on the addition of 30 μM Ca^{2+}. Thus, a strong binding of Ca^{2+} and corresponding change in structure is brought about by PIP_2 alone. Phospholipid cross-linking may serve to stiffen the membrane in areas denuded of proteins, facilitating buckling by synaptotagmin insertion (31). Such a collective, interdependent reorganization of the plasma membrane may then explain the nonlinear Ca^{2+} dependence of vesicle fusion at release sites across the synaptic terminal (22), providing part of the 40–200 k_BT of free energy thought necessary for synaptic vesicle fusion (32,33), and we argue that it should be considered in future schemes of vesicle release.

Further experiments will be needed to fully understand the structural changes that occur in membranes during the fusion reaction. These experiments will need to introduce further complexity in a defined, reproducible manner. First, membranes of a more complex lipid composition (reflecting more accurately the plasma membrane will need to be used. Second, future experiments will also have to consider that proteins participate at multiple stages of the fusion pathway in neurons. For example, synaptotagmin is known to interact with the plasma membrane SNARE proteins syntaxin 1 and SNAP-25, which, together with the vesicular protein synaptobrevin, are thought to constitute the minimal fusion machinery (6,34).

Our choice of a lipid only monolayer was influenced by recent work that suggests that synaptotagmin is responsible for Ca^{2+}-independent docking of the vesicle to PIP_2 at exocytic sites via a polybasic patch on the side of C2B domain, arguably the first stage in the release process (35–37). This is thought to occur separately from its membrane penetration activities, which require reorientation of the C2B domain on the membrane surface.

Unfortunately, the incorporation of SNAREs into artificial membranes usually leads directly to synaptic vesicle fusion, irrespective of Ca^{2+} addition (38). Hence, to fully understand the fusion pathway, syntaxin and SNAP-25 will eventually have to be reconstituted into membranes in a way in which vesicles remain stably associated until Ca^{2+} addition.

SUPPORTING MATERIAL

Details of the preparation methods, experimental parameters, and x-ray analysis are available at http://www.biophysj.org/biophysj/supplemental/S0006-3495(12)00060-4.

We thank Klaus Giewekemeyer for providing the MATLAB tools (The MathWorks, Natick, MA) used to analyze the reflectivity data. We also acknowledge the excellent working conditions at the European Synchrotron Radiation Facility.

This work was financially supported by the Excellence Cluster Initiative 171, Deutsche Forschungsgemeinschaft Research Center 103, Center for Molecular Physiology of the Brain, Functionality Controlled by Organization In and Between Membranes (grant No. SFB803), and the Max Planck Society.

REFERENCES

1. Takamori, S., M. Holt, …, R. Jahn. 2006. Molecular anatomy of a trafficking organelle. *Cell.* 127:831–846.

2. Stein, A., A. Radhakrishnan, …, R. Jahn. 2007. Synaptotagmin activates membrane fusion through a Ca^{2+}-dependent *trans* interaction with phospholipids. *Nat. Struct. Mol. Biol.* 14:904–911.
3. Südhof, T. C. 2004. The synaptic vesicle cycle. *Annu. Rev. Neurosci.* 27:509–547.
4. Jahn, R., T. Lang, and T. C. Südhof. 2003. Membrane fusion. *Cell.* 112:519–533.
5. Aoyagi, K., T. Sugaya, …, M. Takahashi. 2005. The activation of exocytotic sites by the formation of phosphatidylinositol 4,5-bisphosphate microdomains at syntaxin clusters. *J. Biol. Chem.* 280:17346–17352.
6. Chapman, E. R. 2008. How does synaptotagmin trigger neurotransmitter release? *Annu. Rev. Biochem.* 77:615–641.
7. Böckmann, R. A., and H. Grubmüller. 2004. Multistep binding of divalent cations to phospholipid bilayers: a molecular dynamics study. *Angew. Chem. Int. Ed. Engl.* 43:1021–1024.
8. Giner Casares, J. J., L. Camacho, …, J. J. López Cascales. 2008. Effect of Na^{+} and Ca^{2+} ions on a lipid Langmuir monolayer: an atomistic description by molecular dynamics simulations. *ChemPhysChem.* 9:2538–2543.
9. Casillas-Ituarte, N. N., X. Chen, …, H. C. Allen. 2010. Na^{+} and Ca^{2+} effect on the hydration and orientation of the phosphate group of DPPC at air-water and air-hydrated silica interfaces. *J. Phys. Chem. B.* 114:9485–9495.
10. Akutsu, H., and J. Seelig. 1981. Interaction of metal ions with phosphatidylcholine bilayer membranes. *Biochemistry.* 20:7366–7373.
11. Altenbach, C., and J. Seelig. 1984. Ca^{2+} binding to phosphatidylcholine bilayers as studied by deuterium magnetic resonance. Evidence for the formation of a Ca^{2+} complex with two phospholipid molecules. *Biochemistry.* 23:3913–3920.
12. Weygand, M., B. Wetzer, …, M. Lösche. 1999. Bacterial S-layer protein coupling to lipids: x-ray reflectivity and grazing incidence diffraction studies. *Biophys. J.* 76:458–468.
13. Oliveira, R. G., E. Schneck, …, M. Tanaka. 2010. Crucial roles of charged saccharide moieties in survival of Gram negative bacteria against protamine revealed by combination of grazing incidence x-ray structural characterizations and Monte Carlo simulations. *Phys. Rev. E.* 81:041901.
14. McLaughlin, S. 1989. The electrostatic properties of membranes. *Annu. Rev. Biophys. Biophys. Chem.* 18:113–136.
15. Ghosh, S. K., S. Castorph, …, T. Salditt. 2010. In vitro study of interaction of synaptic vesicles with lipid membranes. *N. J. Phys.* 12:105004.
16. Cotman, C., M. L. Blank, …, F. Snyder. 1969. Lipid composition of synaptic plasma membranes isolated from rat brain by zonal centrifugation. *Biochemistry.* 8:4606–4612.
17. Helm, C. A., H. Möhwald, …, J. Als-Nielsen. 1987. Phospholipid monolayer density distribution perpendicular to the water surface. A synchrotron x-ray reflectivity study. *Eur. Phys. Lett.* 4:679–703.
18. Ghosh, S. K., S. Aeffner, and T. Salditt. 2011. Effect of PIP_2 on bilayer structure and phase behavior of DOPC: an x-ray scattering study. *ChemPhysChem.* 12:2633–2640.
19. Cristofolini, L., T. Berzina, …, V. Erokhin. 2007. Structural study of the DNA dipalmitoylphosphatidylcholine complex at the air-water interface. *Biomacromolecules.* 8:2270–2275.
20. Lee, K. Y., A. Gopal, …, K. Kjaer. 2002. Influence of palmitic acid and hexadecanol on the phase transition temperature and molecular packing of dipalmitoylphosphatidyl-choline monolayers at the air-water interface. *J. Chem. Phys.* 116:774–783.
21. Brezesinski, G., A. Dietrich, …, H. Möhwald. 1995. Influence of ether linkages on the structure of double-chain phospholipid monolayers. *Chem. Phys. Lipids.* 76:145–157.
22. Schneggenburger, R., and E. Neher. 2005. Presynaptic calcium and control of vesicle fusion. *Curr. Opin. Neurobiol.* 15:266–274.
23. Herbette, L., C. A. Napolitano, and R. V. McDaniel. 1984. Direct determination of the calcium profile structure for dipalmitoyllecithin multilayers using neutron diffraction. *Biophys. J.* 46:677–685.
24. Schiavo, G., G. Stenbeck, …, T. H. Söllner. 1997. Binding of the synaptic vesicle v-SNARE, synaptotagmin, to the plasma membrane t-SNARE, SNAP-25, can explain docked vesicles at neurotoxin-treated synapses. *Proc. Natl. Acad. Sci. USA.* 3:997–1001.
25. von Poser, C., and T. C. Südhof. 2001. Synaptotagmin 13: structure and expression of a novel synaptotagmin. *Eur. J. Cell Biol.* 80:41–47.
26. Perin, M. S., N. Brose, …, T. C. Südhof. 1991. Domain structure of synaptotagmin (p65). *J. Biol. Chem.* 266:623–629.
27. Martens, S., M. M. Kozlov, and H. T. McMahon. 2007. How synaptotagmin promotes membrane fusion. *Science.* 316:1205–1208.
28. Hui, E., J. Bai, and E. R. Chapman. 2006. Ca^{2+}-triggered simultaneous membrane penetration of the tandem C_2-domains of synaptotagmin I. *Biophys. J.* 91:1767–1777.
29. Paddock, B. E., Z. Wang, …, N. E. Reist. 2011. Membrane penetration by synaptotagmin is required for coupling calcium binding to vesicle fusion in vivo. *J. Neurosci.* 31:2248–2257.
30. Sabatini, B. L., and W. G. Regehr. 1996. Timing of neurotransmission at fast synapses in the mammalian brain. *Nature.* 384:170–172.
31. McMahon, H. T., M. M. Kozlov, and S. Martens. 2010. Membrane curvature in synaptic vesicle fusion and beyond. *Cell.* 140:601–605.
32. Kozlovsky, Y., L. V. Chernomordik, and M. M. Kozlov. 2002. Lipid intermediates in membrane fusion: formation, structure, and decay of hemifusion diaphragm. *Biophys. J.* 83:2634–2651.
33. Siegel, D. P., and M. M. Kozlov. 2004. The Gaussian curvature elastic modulus of *n*-monomethylated dioleoylphosphatidylethanolamine: relevance to membrane fusion and lipid phase behavior. *Biophys. J.* 87:366–374.
34. Weber, T., B. V. Zemelman, …, J. E. Rothman. 1998. SNAREpins: minimal machinery for membrane fusion. *Cell.* 92:759–772.
35. Bai, J., W. C. Tucker, and E. R. Chapman. 2004. PIP_2 increases the speed of response of synaptotagmin and steers its membrane-penetration activity toward the plasma membrane. *Struct. Mol. Biol.* 11:36–44.
36. van den Bogaart, G., S. Thutupalli, …, R. Jahn. 2011. Synaptotagmin-1 may be a distance regulator acting upstream of SNARE nucleation. *Nat. Struct. Mol. Biol.* 18:805–812.
37. Kuo, W., D. Z. Herrick, …, D. S. Cafiso. 2009. The calcium-dependent and calcium-independent membrane binding of synaptotagmin 1: two modes of C2B binding. *J. Mol. Biol.* 387:284–294.
38. Holt, M., D. Riedel, …, R. Jahn. 2008. Synaptic vesicles are constitutively active fusion machines that function independently of Ca^{2+}. *Curr. Biol.* 18:715–722.